Cell Reports, Volume *8*

Supplemental Information

Dysregulated Expression of Neuregulin-1 by Cortical Pyramidal Neurons Disrupts Synaptic Plasticity

Amit Agarwal, Mingyue Zhang, Irina Trembak-Duff, Tilmann Unterbarnscheidt, Konstantin Radyushkin, Payam Dibaj, Daniel Martins de Souza, Susann Boretius, Magdalena M. Brzózka, Heinz Steffens, Sebastian Berning, Zenghui Teng, Maike Gummert, Martesa Tantra, Peter C. Guest, Katrin I. Willig, Jens Frahm, Stefan W. Hell, Sabine Bahn, Moritz J. Rossner, Klaus-Armin Nave, Hannelore Ehrenreich, Weiqi Zhang, and Markus H. Schwab

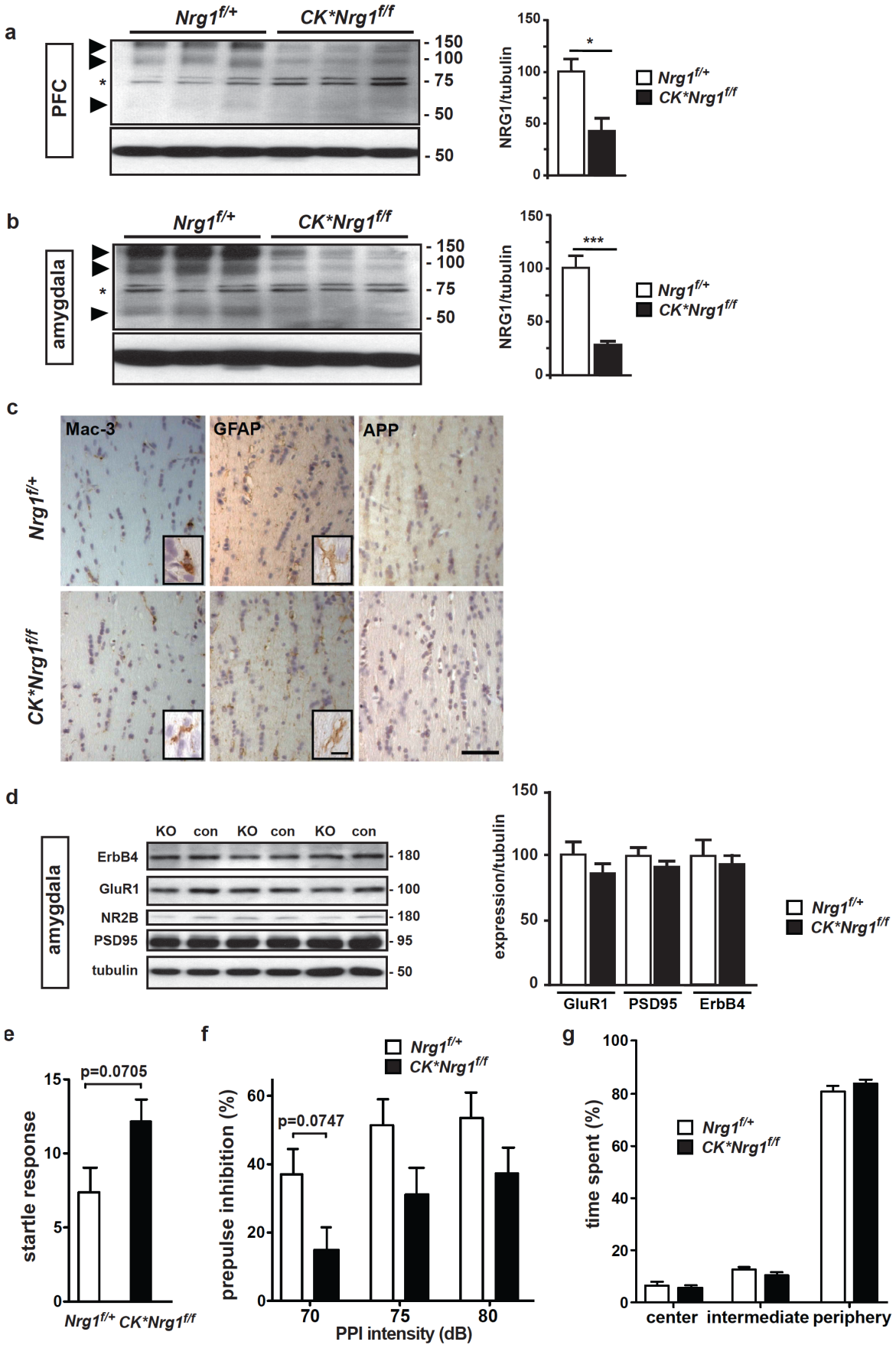
a
Nrg1f/+
CK*Nrg1f/f
PFC
150
100
75
50
50
NRG1/tubulin
*
b
amygdala
***
c
Mac-3
GFAP
APP
Nrg1f/+
CK*Nrg1f/f
d
KO con KO con KO con
ErbB4
GluR1
NR2B
PSD95
tubulin
180
100
180
95
50
expression/tubulin
GluR1
PSD95
ErbB4
e
p=0.0705
startle response
f
p=0.0747
prepulse inhibition (%)
PPI intensity (dB)
70
75
80
g
time spent (%)
center
intermediate
periphery

Supplemental Figures

Figure S1 (related to Figure 1):
Synaptic protein expression in *CK*Nrg1$^{f/f}$* mutants

(a) (left panel) Western blot analysis of protein lysates from prefrontal cortex (PFC) of *CK*Nrg1$^{f/f}$* mutants and *Nrg1$^{f/+}$* controls (age 15 months). Full-length CRD-NRG1 (~140 kDa) and Ig-NRG1 (~95 kDa) isoforms, and a C-terminal processing product (~60 kDa) were reduced in *CK*Nrg1$^{f/f}$* mutants (arrowheads). Asterisk indicates unspecific protein bands. **(right panel)** Densitometric quantification of NRG1 isoforms (140, 95 kDa). 'Integrated density' values were normalized to β-tubulin and are expressed as mean values. (n=3 per genotype; error bars, s.e.m.; *P<0.05; non-parametric, Mann-Whitney U, two-tailed t-test).

(b) (left panel) Western blot analysis of protein lysates from the amygdala (amy) of *CK*Nrg1$^{f/f}$* mutants and *Nrg1$^{f/+}$* controls. **(right panel)** Densitometric quantification of NRG1 isoforms (140; 95; and 60 kDa) as described for PFC. ***P<0.0001. Asterisk indicates unspecific protein bands.

(c) Immunostaining of the corpus callosum for markers of neuroinflammation (Mac3, activated microglia; GFAP, astrogliosis) and neurodegenration (APP, axonal swellings) on coronal brain sections from *CK*Nrg1$^{f/f}$* mutants and *Nrg1$^{f/+}$* controls (age 12 months). Sections were counterstained with hematoxylin. Scale bars, 50 µm; 10 µm (insets).

(d) (left panel) Western blot analysis of protein extracts from the amygdala of *CK*Nrg1$^{f/f}$* mutants and *Nrg1$^{f/+}$* controls after treatment with MK-801 (age 15 months). **(right panel)** Densitometric quantification as in (a).

(e, f) *CK*Nrg1$^{f/f}$* mice at 3-4 months show a tendency for an increased startle response (p=0.0705, Mann-Whitney U-test) and decreased pre-pulse inhibition of the startle response at 70 dB (effect of genotype $F_{1\text{-}44}$=3.5, p=0.0747, 2-way ANOVA for repeated measures).

(g) The fraction of time *CK*Nrg1$^{f/f}$* mutants spent in different zones of the open-field arena was similar for *CK*Nrg1$^{f/f}$* mutants and *Nrg1$^{f/+}$* controls.

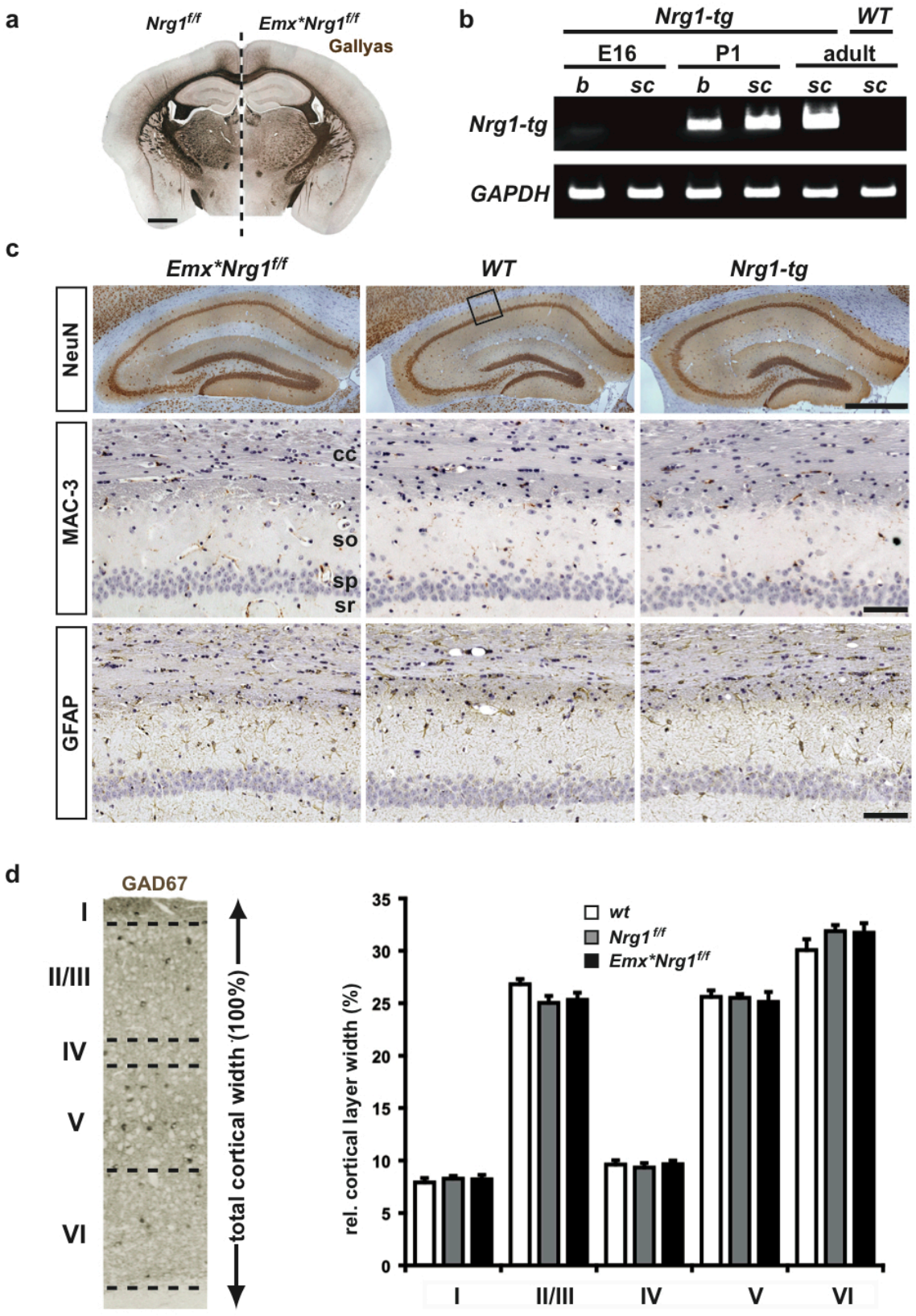
a
Nrg1f/f
Emx*Nrg1f/f
Gallyas
b
Nrg1-tg
WT
E16
P1
adult
b
sc
b
sc
sc
sc
Nrg1-tg
GAPDH
c
Emx*Nrg1f/f
WT
Nrg1-tg
NeuN
MAC-3
cc
so
sp
sr
GFAP
d
GAD67
I
II/III
IV
V
VI
total cortical width (100%)
rel. cortical layer width (%)
wt
Nrg1f/f
Emx*Nrg1f/f
35
30
25
20
15
10
5
0
I
II/III
IV
V
VI

Figure S2 (related to Figure 3):

Histology of *Emx*Nrg1*$^{f/f}$ mutants and *Nrg1-tg* mice

(a) Normal white matter structures and subcortical axonal projections in *Emx*Nrg1*$^{f/f}$ mutants compared to *Nrg1*$^{f/f}$ controls. Myelin staining (Gallyas silver impregnation) of coronal brain sections (age 3 months). Scale bar, 1mm.

(b) Onset of transgene expression in *Nrg1-tg* mice during late embryonic stages. RT-PCR with transgene-specific primers on brain (b) and spinal cord (sc) cDNA prepared from *Nrg1-tg* mice and *WT* at indicated stages. Note weak transgene expression in E16 brain. Amplification of GAPDH was used as an internal control.

(c) No signs of neurodegeneration and neuroinflammation in the hippocampus of *Emx*Nrg1*$^{f/f}$ mutants and *Nrg1-tg* mice. Immunostaining for neurons (NeuN) and markers of neuroinflammation (Mac3, activated microglia; GFAP, astrogliosis; higher magnification of CA1 region boxed in *WT* NeuN staining) on coronal brain sections from *Emx*Nrg1*$^{f/f}$ mutants, *Nrg1-tg* mice and *WT* (age 12 months). Abbreviations: cc, corpus callosum; so, stratum oriens; sp, stratum pyramidale; sr, stratum radiatum. Scale bars, 500 µm (top); 150 µm (middle and bottom).

(d) Normal cortical lamination in *Emx-Nrg1*$^{f/f}$ mutants and *Nrg1-tg* mice. Relative cortical layer width was determined based on GAD67 immunoreactivity on coronal brain sections (left panel, representative micrograph from *Nrg1*$^{f/f}$ mice, bregma -1.7; n=6 per genotype).

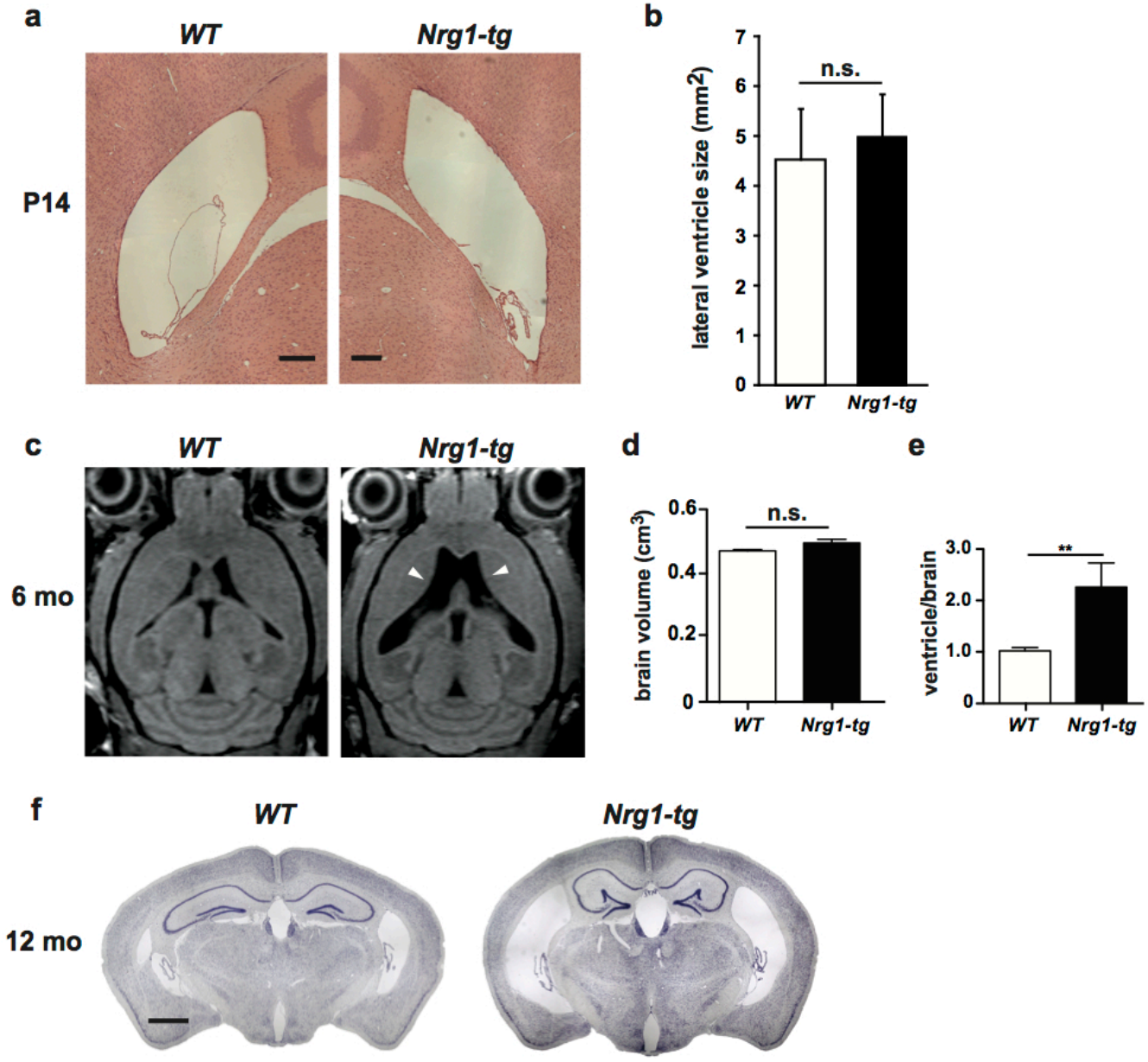
a
WT
Nrg1-tg
P14
b
lateral ventricle size (mm2)
n.s.
WT
Nrg1-tg
c
WT
Nrg1-tg
6 mo
d
brain volume (cm3)
n.s.
WT
Nrg1-tg
e
ventricle/brain
**
WT
Nrg1-tg
f
WT
Nrg1-tg
12 mo

Figure S3 (related to Figure 4):
Ventricular enlargement in adult *Nrg1-tg* mice

(a) Hematoxylin and Eosin staining of coronal brain sections (bregma -1.7) of *WT* and *Nrg1-tg* mice at P14. Scale bar, 200 μm.

(b) Lateral ventricles were not increased in *Nrg1-tg* compared to *WT* mice at P14. Ventricular size (bregma -1.7) was quantified on microscopic pictures (10x) using ImageJ (n=6 per genotype; error bars, s.e.m.; P=0.6991; non-parametric two-tailed t-test; ns, not significant).

(c) Enlarged lateral ventricles (white arrowheads) in *Nrg1-tg* compared to *WT* mice at 6 months (T1-weighted *in vivo* MRI).

(d) Volumetric analysis shows normal total brain volume (cm^3) in *Nrg1-tg* mice compared to *WT* (age 6 months; n=6 per genotype; error bars, s.e.m.; P=0.31; non-parametric two-tailed t-test; ns, not significant).

(e) Ventricular volume (percentage of total brain volume**)** is increased in *Nrg1-tg* mice compared to *WT*. *(n=5*, *WT*; n=4, *Nrg1-tg* mice; error bars, s.e.m.; **P<0.01; non-parametric two-tailed t-test).

(**f**) Enlarged lateral ventricles in *Nrg1-tg* mice at 12 months (Nissl staining of coronal brain sections). Note that ventricular enlargement results in deformation of the hippocampus. Scale bar, 1 mm.

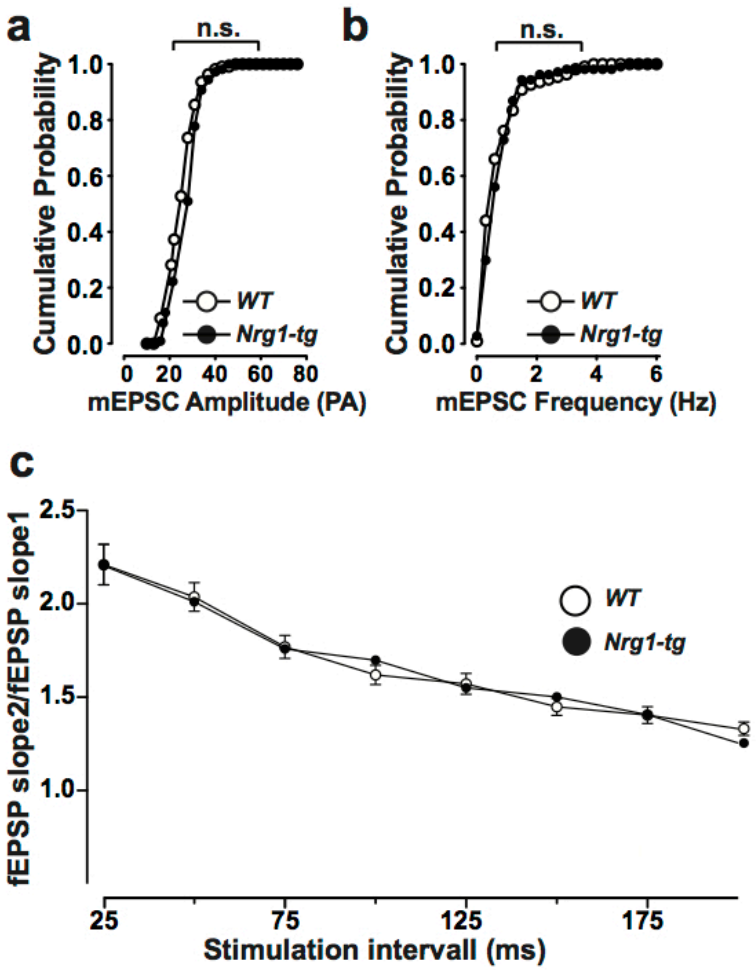

Figure S4 (related to Figure 5):

Elevated CRD-NRG1 expression has no effect on basal synaptic transmission and mEPSCs in CA1 pyramidal neurons

(a, b) Averaged mEPSC amplitude (a) and frequency (b) in pyramidal neurons from *Nrg1-tg* mice (n=15) were not changed compared to WT (n=10).

(c) Paired-pulse ratio at inter-stimulus intervals of 25–75 ms was unchanged in *Nrg1-tg* mice compared to WT.

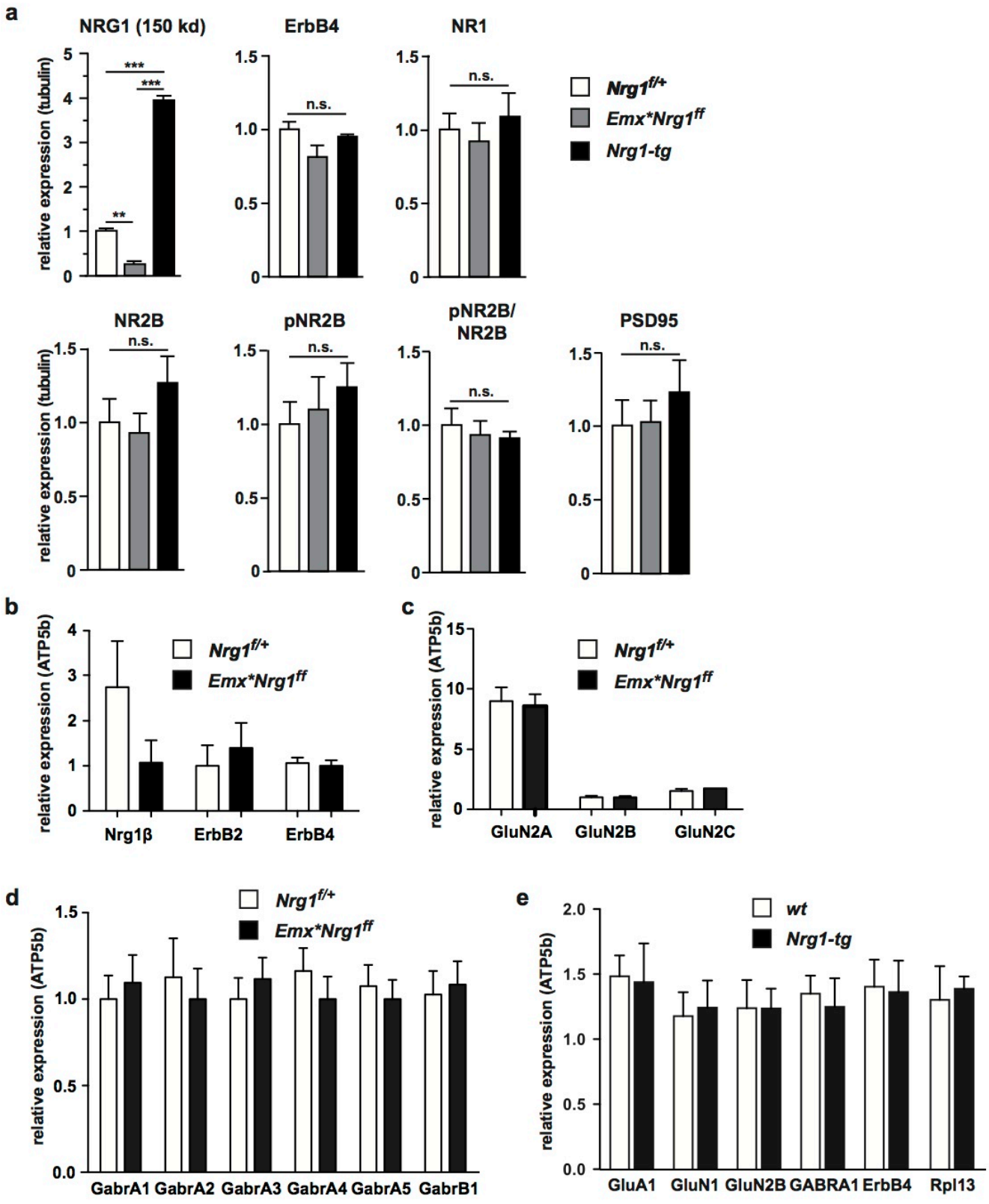
a
NRG1 (150 kd)
ErbB4
NR1
relative expression (tubulin)
***
***
**
n.s.
n.s.
Nrg1f/+
Emx*Nrg1ff
Nrg1-tg
NR2B
pNR2B
pNR2B/ NR2B
PSD95
b
relative expression (ATP5b)
Nrg1β
ErbB2
ErbB4
c
GluN2A
GluN2B
GluN2C
d
GabrA1
GabrA2
GabrA3
GabrA4
GabrA5
GabrB1
e
wt
GluA1
GluN1
GluN2B
GABRA1
ErbB4
Rpl13

Figure S5 (related to Figure 5):

Expression of neurotransmitter receptors in *Emx*Nrg1*$^{f/f}$ mutants and *Nrg1-tg* mice

(a) Densitometric quantification of proteins isolated from synaptic plasma membranes (TritonX-100 soluble and insoluble fractions) of *Emx*Nrg1*$^{f/f}$ mutants, *Nrg1-tg* mice, and *Nrg1*$^{f/+}$ controls. NRG1 was extracted from the TritonX-100 soluble fraction, all other proteins were solubilized in SDS-buffer from the postsynaptic density fraction. 'Integrated density' values were normalized to β-tubulin and expressed as mean values. (n=3 per genotype; error bars, s.e.m.; **P<0.01, ***P<0.001: one way ANOVA with post-hoc Tukey's multiple comparision test).

(b-d) Quantitative RT-PCR on pooled cDNA from the hippocampus of *Emx*Nrg1*$^{f/f}$ mutants (n=8) and controls (*Nrg1*$^{f/+}$, n=8) (age 4-5 months). **(a)** NRG1β expression was reduced by 70% in *Emx*Nrg1*$^{f/f}$ mutants (similar to NRG1 protein levels, see Fig. 3b), in contrast expression of ErbB2 and ErbB4 was not altered in *Emx*Nrg1*$^{f/f}$ mutants. **(b)** Expression of NMDA receptor 2 subunits A (GluN2A), B (GluN2B), C (GluN2C) and **(c)** all five subunits of GABAaα **(**GabrA1, GabrA2, GabrA3, GabrA4, GabrA5) and GABAaβ1 (GabrB1) receptors was unchanged in *Emx*Nrg1*$^{f/f}$ mutants compared to controls. Amplification of the housekeeping gene ATP5b was used for relative quantification.

(e) Quantitative RT-PCR on pooled cDNA from the hippocampus of *Nrg1-tg mice* (n=6) and wildtype mice (*WT,* n=6) (age 10-11 months). Expression of mRNAs for ionotropic glutamate receptors (AMPA receptor subunit 1, GluA1; NMDA receptor subunit 1, GluN1; subunit 2B, GluN2B), ionotropic GABA receptor (GABAa receptor α1; GABRA1) and ErbB4 receptor was similar in *Nrg1-tg* and *WT* mice. The housekeeping gene ribosomal protein L13 (Rpl13) was used as a quality control. Amplification of the housekeeping gene ATP5b was used for relative quantification.

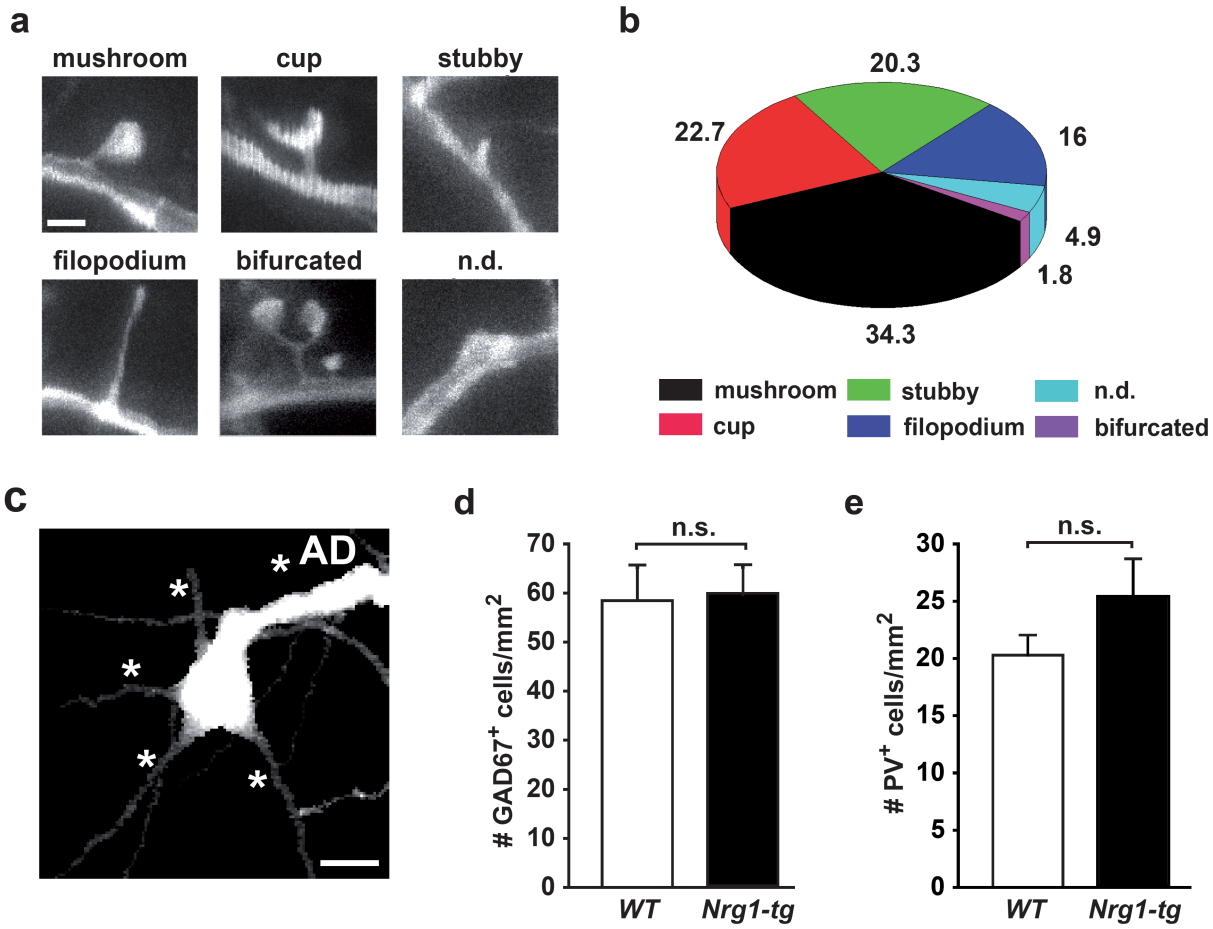

Figure S6 (related to Figure 6):

***In vivo* imaging of *CRD-Nrg1* transgenic mice**

(a) Representative examples of morphological spine classes in the MZ of 3 months old *Thy1.2-YFP* mice obtained by *in vivo* STED nanoscopy of dendrites derived from cortical layer V projection neurons. Scale bar, 1 µm.

(b) Frequency (in %) of spine classes in the MZ of *Thy1.2-YFP* mice (averaged values from n=4 mice, 30 dendrites/mouse; n.c., not classified).

(c) Primary dendrites (labeled by asterisks; AD, apical dendrite) emerging from layer V projection neuron marked by white box in Fig. 6a. Scalebar, 20 µm.

(d) Number of $GAD67^+$ interneurons in the hippocampus of *Nrg1-tg* mice and *WT* at P14 (Bregma, -1.7, both hemispheres; n=6 mice per genotype, n.s., not significant).

(e) Number of PV^+ interneurons in the hippocampus of *Nrg1-tg* mice and *WT* at P14 (Bregma, -1.7, both hemispheres; n=6 mice per genotype, n.s., not significant).

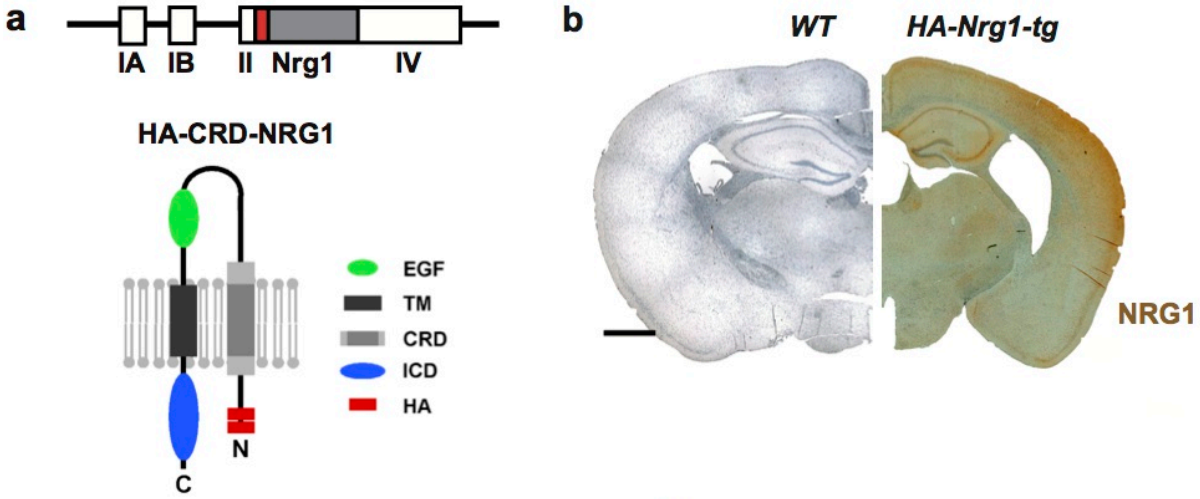
a
IA
IB
II
Nrg1
IV
HA-CRD-NRG1
EGF
TM
CRD
ICD
HA
N
C
b
WT
HA-Nrg1-tg
NRG1

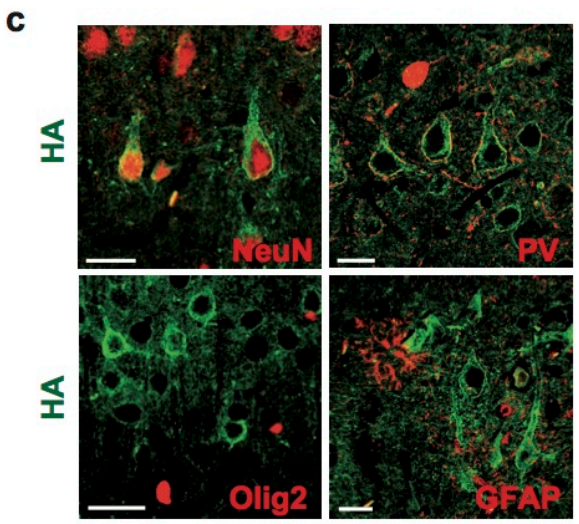
c
HA
NeuN
PV
HA
Olig2
GFAP

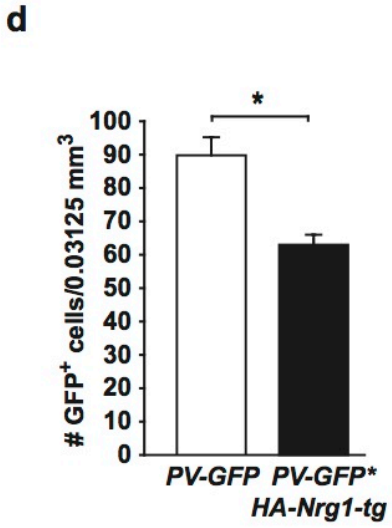
d
*
GFP+ cells/0.03125 mm3
100
90
80
70
60
50
40
30
20
10
0
PV-GFP
PV-GFP*
HA-Nrg1-tg

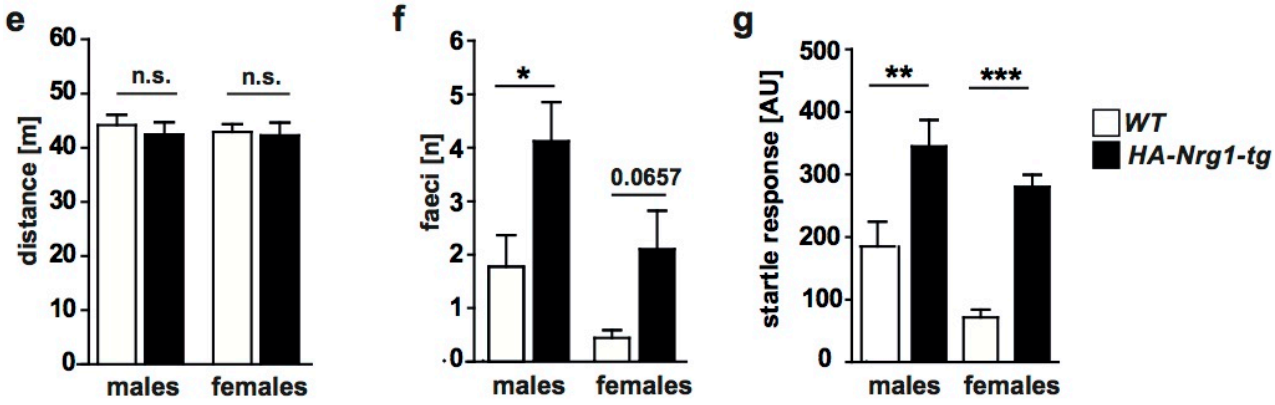
e
distance [m]
60
50
40
30
20
10
0
n.s.
n.s.
males
females
f
faeci [n]
6
5
4
3
2
1
0
*
0.0657
males
females
g
startle response [AU]
500
400
300
200
100
0
**
***
males
females
WT
HA-Nrg1-tg

Figure S7 (related to Figure 7):

Expression analysis and behavioral characterization of *HA-Nrg1-tg* mice

(a) (upper panel) Structure of the Thy1.2 transgene cassette (red box, HA epitope; grey box, full-length CRD-Nrg1 cDNA; white boxes, exons I-IV of the Thy1.2 gene). (lower panel) In HA-CRD-NRG1 two HA epitope tags are located at the N-terminus of CRD-NRG1. CRD, cystein-rich domain; EGF, epidermal growth factor-like domain; HA, HA epitope tag; ICD, intracellular domain; TM, transmembrane domain.

(b) Chromogenic NRG1 immunostaining (ICD domain) on coronal brain sections from wildtype (*WT*) and HA-CRD-NRG1 expressing transgenic mice (*HA-Nrg1-tg*) at 4 months of age. Note enlarged lateral ventricle in *HA-Nrg1-tg* brain, similar to *Nrg1-tg* mice. Scalebar, 1 mm.

(c) Fluorescent immunostaining for the HA epitope and cell type-specific markers (neurons, NeuN; interneurons, PV; oligodedrocytes, Olig2; astrocytes, GFAP) on coronal brain sections from *HA-Nrg1-tg* mice (age 4 months). Scalebars, 25 µm (PV, 20 µm).

(d) Number of GFP^+ interneurons in a cortical column of 250*250*500 µm (0.03125 mm^3) of *PV-GFP*HA-Nrg1-tg* mice (n=2) and *PV-GFP* controls (n=5) obtained by *in vivo* two-photon imaging (*P<0.05).

(e) Distance travelled in the open-field test was similar in *HA-Nrg1-tg* and *WT* mice of both sexes (age 2-3 months, males: p=0.5575, females p=0.6835; Mann-Whitney test).

(f) Male *HA-Nrg1-tg* mice showed more frequent defecation compared to *WT* mice during the open-field test (P=0.0129; Mann-Whitney test); a similar tendency (P=0.0657) was observed for female *HA-Nrg1-tg* mice.

(g) *HA-Nrg1-tg* mice (males: P=0.0083; females: P<0.0001; Mann-Whitney test) displayed increased startle response to a 120 dB pulse in the prepulse inhibition test. (*WT* mice: males, n=18; females, n=18; *HA-Nrg1-tg* mice: males, n=16; females, n=10. Error bars ± s.e.m. *P <0.05; **P<0.01; ***P<0.001; n.s., not significant; Mann-Whitney U-test. AU, arbitrary units).

Supplemental Tables

Biological Process	Gene	Accession	Protein Description	Molecular function	MW	Ratio	FC	ID Pep	Wilcoxon	t-test	q value
Cell comm. and signalling	Camk2a	KCC2A_MOUSE	Ca+2/calmodulin-dependent protein kinase type II alpha chain	Protein serine/threonine kinase activity	54115	0,67	-1,49	51	0,0304	0,0407	0,2665
	Camk2b	KCC2B_MOUSE	Ca+2/calmodulin-dependent protein kinase type II beta chain	Protein serine/threonine kinase activity	60461	0,77	-1,30	43	0,0304	0,0273	0,2665
	Eef1d	EF1D_MOUSE	Elongation factor 1-delta	Guanyl-nucleotide exchange factor activity	31293	0,81	-1,23	2	0,0141	0,0109	0,3952
	Gna14	GNA14_MOUSE	Guanine nucleotide-binding protein subunit alpha-14	GTPase activity	41528	0,90	-1,11	8	0,0304	0,0174	0,3952
	Hcls1	HCLS1_MOUSE	Hematopoietic lineage cell-specific protein	Molecular function unknown	54240	1,09	1,09	3	0,0141	0,0095	0,2665
	Mapk1	MK01_MOUSE	Mitogen-activated protein kinase 1	Protein serine/threonine kinase activity	41276	0,92	-1,08	33	0,0464	0,0449	0,3952
	Mrc1	MRC1_MOUSE	Macrophage mannose receptor 1	Receptor activity	164981	1,29	1,29	2	0,0194	0,0417	0,3952
	Omg	OMGP_MOUSE	Oligodendrocyte-myelin glycoprotein	Cell adhesion molecule activity	49284	0,79	-1,26	5	0,0073	0,0155	0,2665
	Phb	PHB_MOUSE	Prohibitin	Receptor signaling complex scaffold activity	29820	0,89	-1,12	35	0,0404	0,0345	0,3952
	Pld2	PLD2_MOUSE	Phospholipase D2	Phospholipase activity	106168	1,43	1,43	2	0,0304	0,0465	0,3952
	Ppp3cc	PP2BC_MOUSE	Ser/Thr-protein phosphatase 2B catalytic subunit gamma	Protein serine/threonine phosphatase activity	58699	1,23	1,23	6	0,0141	0,0057	0,3952
	Rab8a	RAB8A_MOUSE	Ras-related protein Rab-8A	GTPase activity	23668	1,19	1,19	16	0,0404	0,0291	0,3952
	Sh3gl2	SH3G2_MOUSE	Endophilin-A1	Molecular function unknown	39955	0,87	-1,15	6	0,0464	0,0323	0,2665
	Stip1	STIP1_MOUSE	Stress-induced-phosphoprotein 1	Receptor signaling complex scaffold activity	62582	0,72	-1,40	2	0,0351	0,0199	0,3952
Cell growth/maintenance	Actr1b	ACTY_MOUSE	Beta-centractin	Structural constituent of cytoskeleton	42281	0,90	-1,11	2	0,0464	0,0346	0,2665
	Dctn2	DCTN2_MOUSE	Dynactin subunit 2	Motor activity	44117	0,77	-1,30	3	0,0102	0,0042	0,2665
	Map1a	MAP1A_MOUSE	Microtubule-associated protein 1A	Cytoskeletal protein binding	30014	1,10	1,10	37	0,0304	0,0406	0,3952
	Tnr	TENR_MOUSE	Tenascin-R	Extracellular matrix structural constituent	149589	0,91	-1,10	86	0,0120	0,0045	0,2665
	Vcan	CSPG2_MOUSE	Versican core protein	Extracellular matrix structural constituent	366787	0,80	-1,25	2	0,0043	0,0012	0,2665
	Actr2	ARP2_MOUSE	Actin-related protein 2	Structural constituent of cytoskeleton	44761	0,89	-1,13	23	0,0464	0,0429	0,3952
Immune response	Mog	MOG_MOUSE	Myelin-oligodendrocyte glycoprotein	Antigen binding	28271	0,78	-1,29	13	0,0061	0,0050	0,3952
Energy Metabolism	Ak4	KAD4_MOUSE	Adenylate kinase isoenzyme 4, mitochondrial	Catalytic activity	25062	0,84	-1,19	7	0,0226	0,0175	0,3952
	Ahcy11	SAHH2_MOUSE	Putative adenosylhomocysteinase 2	Hydrolase activity	58951	0,71	-1,42	4	0,0120	0,0135	0,3952
	Apeh	APEH_MOUSE	Acylamino-acid-releasing enzyme	Hydrolase activity	81522	1,22	1,22	3	0,0351	0,0203	0,2665
	Gpi	G6PI_MOUSE	Glucose-6-phosphate isomerase	Isomerase activity	62767	0,73	-1,37	86	0,0262	0,0464	0,2665
	Phka1	KPB1_MOUSE	Phosphorylase b kinase regulatory subunit alpha	Phosphorylase activity	138825	0,70	-1,43	2	0,0194	0,0347	0,2665
	Prdx3	PRDX3_MOUSE	Thioredoxin-dependent peroxide reductase, mitochondrial	Peroxidase activity	28127	1,14	1,14	12	0,0194	0,0393	0,3952
	Psat1	SERC_MOUSE	Phosphoserine aminotransferase	Transaminase activity	40473	0,78	-1,28	14	0,0226	0,0245	0,3952
	Qdpr	DHPR_MOUSE	Dihydropteridine reductase	Catalytic activity	25570	0,78	-1,28	19	0,0304	0,0269	0,3952
	Tecr	GPSN2_MOUSE	Synaptic glycoprotein SC2	Catalytic activity	36090	0,87	-1,15	2	0,0464	0,0389	0,2665
Regulation of cell cycle	Eef1a1	EF1A1_MOUSE	Elongation factor 1-alpha 1	Transcription regulator activity	50114	0,62	-1,61	29	0,0166	0,0321	0,2665
Reg. of nucleic acid metab.	Aco1	ACOC_MOUSE	Cytoplasmic aconitate hydratase	Isomerase activity	98126	1,16	1,16	4	0,0141	0,0163	0,3952
	Ddx5	DDX5_MOUSE	Probable ATP-dependent RNA helicase DDX5	RNA binding	69290	1,13	1,13	5	0,0194	0,0083	0,2665
	Lrpprc	LPPRC_MOUSE	Leucine-rich PPR motif-containing protein, mitochondrial	RNA binding	156615	1,11	1,11	7	0,0464	0,0362	0,2665
	Prpsap2	KPRB_MOUSE	Phosphoribosyl pyrophosphate synthetase-associated protein 2	Molecular function unknown	40881	0,81	-1,23	5	0,0073	0,0026	0,3952
Transport	Atp1b1	AT1B1_MOUSE	Sodium/potassium-transporting ATPase subunit beta-1	ATPase activity	35195	0,80	-1,25	31	0,0226	0,0186	0,2665
	Pacs1	PACS1_MOUSE	Phosphofurin acidic cluster sorting protein 1	Receptor signaling complex scaffold activity	104829	1,13	1,13	3	0,0404	0,0314	0,2665
	Slc12a6	S12A6_MOUSE	Solute carrier family 12 member 6	Auxiliary transport protein activity	127527	1,15	1,15	19	0,0120	0,014	0,2665
	Slc4a10	S4A10_MOUSE	Sodium-driven chloride bicarbonate exchanger	Auxiliary transport protein activity	125817	1,27	1,27	8	0,0262	0,0373	0,2665
Unknown	Sept6	SEPT6_MOUSE	Septin-6;	Molecular function unknown	49620	0,86	-1,17	2	0,0464	0,0386	0,2665

Table S1 (related to Figure 5):

Differentially expressed proteins in the hippocampus of *Nrg1-tg* mice

Proteins with differential expression between *Nrg1-tg* and *WT* mice were identified by LC-MSE as described in the methods section. Indicated are the biological processes, gene names (gene), UniProt accession codes, protein description, molecular function, molecular weight (MW), ratio (*Nrg1-tg*/*WT*), number of peptides identified (ID pep), Wilcoxin, t-test and q-values for each protein.

Gene name	Accession	Protein description
GRIN1	Q05586	Glutamate [NMDA] receptor subunit zeta-1
GRIN2B	Q13224	Glutamate [NMDA] receptor subunit epsilon-2
GRIN2A	Q12879	Glutamate [NMDA] receptor subunit epsilon-1
GRIK2	Q13002	Glutamate receptor, ionotropic kainate 2
GRIA1	P42261	Glutamate receptor AMPA 1
ITPR1	Q14643	Inositol 1,4,5-trisphosphate receptor type 1
AHCYL1	Q2NKW8	Adenosylhomocysteinase
NOS1	P29475	Nitric oxide synthase, brain
RARA	P10276	Retinoic acid receptor alpha
FMR1	Q06787	Fragile X mental retardation protein 1
HTT	P42858	Huntingtin
NSF	P46459	Vesicle-fusing ATPase
DLG1	Q12959	Disks large homolog 1
DLG2	Q15700	Disks large homolog 2
DLG4	P78352	Disks large homolog 4
ATP5B	P06576	ATP synthase subunit beta, mitochondrial
SNAP25	P60880	Synaptosomal-associated protein 25
STX1A	Q16623	Syntaxin-1A
STXBP1	P61764	Syntaxin-binding protein 1
KCNA2	P16389	Potassium voltage-gated channel subfamily A member 2
VCAM1	P19320	Vascular cell adhesion molecule 1
IL6	IP05231	Interleukin-6
APP	P05067	Amyloid beta A4 protein

Table S2 (related to Figure 5):

"Interactom" of differentially expressed proteins in *Nrg1-tg* mice

List of proteins in the IPKB database known to interact with the uploaded proteins from Table S1. The table gives the gene name, accession code and protein description.

Table S3: Summary of "endophenotypes" in transgenic mice overexpressing various *neuregulin1* isoforms.

Endophenotype	Full-length CRD-NRG1 [a]	Full-length Ig-NRG1 [b]	Full-length Ig-NRG1 [c]	BACE1-processed Ig-NRG1 [d]
interneuron migration/numbers	Reduced PV+ interneurons	*nd*	unchanged	*nd*
spines	abnormal growth	*nd*	*nd*	*nd*
LTP	reduced	unchanged	*nd*	*nd*
glutamatergic neurotransmission[1]	unchanged	unchanged[2]	reduced EPSC frequency	*nd*
GABAergic neurotransmission[1]	increased IPSC frequency	reduced γ- oscillation	reduced IPSC amplitude	*nd*
ventricular size	increased	unchanged[3]	*nd*	*nd*
motor activity (open field)	unchanged	increased	increased	increased
PPI	reduced	*nd*	reduced	unchanged

[a]current study, **[b]Deakin et al., 2011**, **[c]Yin et al., 2013**, **[d]Luo et al., 2013**

[1]glutamatergic projection neurons, [2]paired pulse facilitation, [3]personal communication, nd: not determined

Table S4: Summary of "endophenotypes" in NRG1

mouse mutants of various *neuregulin1* isoforms.

Endophenotype	*CamKII*Nrg1$^{f/f}$* [a]	*CRD-Nrg1$^{+/-}$* [b]	*Ig-Nrg1$^{+/-}$* [c]	*Nrg1$^{+/-}$* [d]
interneuron migration/numbers	unchanged	*nd*	*nd*	*nd*
spines	*nd*	reduced spine density	*nd*	*nd*
LTP	reduced	reduced[2]	*nd*	increased
glutamatergic neurotransmission	reduced mEPSC (amplitude only)	mEPSC unchanged[3]	*nd*	*nd*
GABAergic neurotransmission	increased mIPSC (amplitude only)[1]	*nd*	*nd*	*nd*
ventricular size	reduced	increased	*nd*	*nd*
motor activity (open field)	reduced	unchanged	unchanged	increased
PPI	reduced	reduced	unchanged	reduced

[a]current study, **[b]Chen et al., 2008; Jiang et al., 2013**, **[c]Rimer et al., 2005; Rao et al., 2004**, **[d]O'Tuathaigh et al., 2010; Stefansson et al., 2002**, **Gerlai et al., 2000; Shamir et al., 2012**.

[1]CA1 pyramidal neurons, [2]cortical–BLA synapses, [3]BLA pyramidal neurons

Supplemental Experimental Procedure.

Protein analysis. Protein lysates were prepared using an Ultraturrax (T8). Tissues were homogenized in 1 ml of modified RIPA buffer (50 mM Tris-HCl pH 7.4, 150 mM NaCl, 1 mM EDTA, 0.1% SDS, 1% TritonX-100, 1% Sodium deoxycholate, 1 mM PMSF and 1 mM Sodium vanadate) and protease inhibitors (Complete tablets, Roche). To study ErbB4 phosphorylation, protein lysates were prepared using sucrose lysis buffer (320 mM Sucrose, 10 mM Tris pH7,4, 1 mM $NaHCO_3$, 1 mM $MgCl_2$) complemented with Roche Protease Inhibitor complete plus mini and Roche PhoSTOP phosphatase inhibitor. For Western Blotting 1-5 µg [50 µg, for NRG1] of cortical or total brain lysate was size-separated on 8% SDS-polyacrylamide gels and blotted onto PVDF membranes (Hybond™-P) following instructions from Invitrogen. Membranes were blocked in 5% milk powder prepared in TBS buffer (50 mM Tris-HCl, pH 7.4 and 150 mM NaCl) for 1-2 hours at room temperature. Primary antibodies directed against GluR1 (pRb, 1:1000, Chemicon), NMDAR1 (mM, 1:7000, Synaptic systems), NMDAR2B (pRb, 1:2000, Chemicon), pErbB4 (mM, 1:1000, Cell Signaling), NRG1 (Sc-348, pRb, 1:500, Santa Cruz Biotechnology), nAchα7 (mM, 1:1000, Covance), PSD95 (mM, 1:10000, Upstate), β-actin (mM, 1:1000, Millipore) and tubulin (mM, 1:2000, Sigma) were diluted in blocking buffer and incubated overnight at 4°C. Membranes were washed three times (10 min each) in TBS-T buffer (50 mM Tris-HCl, pH 7.4, 150 mM NaCl and 0.05% Tween-20), followed by an incubation with a horseradish peroxidase-conjugated secondary antibody (diluted 1:5,000-10,000 in blocking buffer). After 5 additional wash steps (10 min each) with TBS-T buffer, proteins were detected with an enhanced chemiluminescence kit (Western Lightning™, Western Blot Chemiluminescence Reagent Plus, PerkinElmer Life Sciences, Inc.) according to the manufacturer's instructions. Exposure of ECL films (Hyperfilm™, Amersham Biosciences) was carried out varying from 10 seconds to 15 minutes depending upon signal intensity. Films were scanned. The densitometric analysis of scanned ECL films was carried out using ImageJ (NIH). The peak intensity value for the band of interest calculated by ImageJ was normalized to the peak intensity value of tubulin. The normalized values (±SEM) were depicted as histograms using GraphPad Prism 5.0.

Synaptosomes and synaptic plasma membrane preparation. The protocol used in this study involves the preparation of isolated nerve terminals (synaptosomes) by a sucrose density gradient technique **(Dodd et al., 1981)**. We modified this technique to rapidly isolate synaptosomes from very small quantities of starting material (such as cerebral cortices and hippocampi microdissected from two mouse brains). Synaptosomes isolated by this technique were lysed in Tris-HCl buffer (pH 8.0) to obtain crude synaptic plasma membranes (SPM), which were fractionated into Triton X-100 soluble and insoluble fraction by ultra-centrifugation **(Mizoguchi et al., 1989)**. The detailed steps for the preparation of crude synaptosomal membrane are as follows. Mice were sacrificed by cervical spinal cord dislocation and were decapitated. Brains were instantly removed and were micro dissected in chilled 1X Phosphate buffered saline (PBS) to isolate forebrain by cutting out olfactory bulb, midbrain, hindbrain and cerebellum. Each dissected forebrain was further separated into cerebral cortex and hippocampus, which were independently prepared for synaptosomal isolation. Cerebral cortices obtained from two mice were placed into a glass potter containing 1.5 ml of homogenization buffer (0.32 mM Sucrose in 4 mM HEPES buffer at pH 7.3) and was gently homogenized using a glass-Teflon homogenizer (16 up/down strokes, 900 rpm). The pistil was further rinsed with 1.5 ml of homogenization buffer for complete recovery of homogenate. The homogenate was centrifuged at 1000_{gmax} for 10 min at 4ºC. The resulting pellet containing large cell fragments and nuclei was discarded and the supernatant was collected. The supernatant (0.32 M) was gently placed on the 0.8 M layer of the sucrose gradient that was prepared by layering 3.0 ml sucrose solutions of following concentrations: 1.2 M (lowermost), 1.0 M, 0.8 M. The resultant sucrose gradient was centrifuged at 110,000 $_{gmax}$ for 2 hours at 4ºC to separate brain lysates into various sub-cellular fractions. Relatively pure fraction of synaptosomes (~50% purity) was obtained from the interface between 1.0 M and 1.2 M sucrose. Further on synaptosomes were diluted in 3.5 ml of homogenization buffer and pelleted by centrifugation at 37,000 $_{gmax}$ for 20 min at 4ºC. The pelleted synaptosomes were lysed by osmotic shock in 1.8ml of 4 mM HEPES buffer (pH 7.4) and centrifuged at 37,000 $_{gmax}$ for 20 min at 4ºC

to get crude synaptic membranes (SPMs). SPMs were further fractionated into Triton X-100 buffer (6 mM Tris-HCl, 1.0% TritonX-100 (pH 8.0)) soluble and insoluble fraction by centrifugation at $135{,}000_{gmax}$ for 20 min at 4ºC. The supernatant (i.e. TritonX-100 soluble fraction) is solubilized synaptic membranes. TritonX-100 insoluble fraction (PSD fraction), mainly consisting of post-synaptic density proteins was solubilized using SDS buffer (2% Sodium dodecyl sulfate, 5% 2-mercaptoethanol in 50 mM Tris-HCl, pH 7.4). The composition of synaptic protein in TritonX-100 soluble and insoluble fractions were analysed using SDS-PAGE and by western blotting as described above, and following primary antibodies were used: ErbB4 (Sc-283, pRb, 1:1000, Santa Cruz Biotechnology), NMDAR1 (mM, 1:7000, Synaptic systems), NMDAR2B (pRb, 1:2000, Chemicon), phosphorylated NMDAR2B (pRb, 1:1000, Chemicon), NRG1 (Sc-348, pRb, 1:500, Santa Cruz Biotechnology), PSD95 (mM, 1:10000, Upstate) and tubulin (mM, 1:2000, Sigma).

Histology and immunostaining. Mice were anesthetized with avertin and perfused with 4% PFA in 0.1 M Phosphate buffer. Brains were postfixed in 4% PFA for one hour to overnight at 4°C. After post-fixation tissues were either embedded in paraplast or stored in 1% PFA in 0.1 M PBS at 4°C until further processed. Free-floating vibratome (40-50 µm) or paraffin sections (5 µm) were incubated overnight with primary antibodies directed against CNP (mM, 1:150, Sigma), GAD67 (mM, 1:1000, Chemicon), GFAP (pRb, 1:200, DAKO; mM, 1:500, Chemicon), HA epitope (mM, 1:250, Covance; pRb, 1:500, Abcam), MAP2 (mM, 1:1000, Sigma), NeuN, mM, 1:200, Chemicon), NRG1 (Sc-348, pRb, 1:500, Santa Cruz Biotechnology), Olig2 (pRb, 1:200, John Alberta, Harvard), PV (pRb, 1:200, Swant). Sections were further incubated with secondary antibodies Cy2 (1:10000, Jackson ImmunoResearch), Cy3 (1:10000, Jackson ImmunoResearch), Alex-488 and Alexa 555 (1:2000, Invitrogen) for 1 hour at room temperature. For the analysis of neurodegenerative changes and cell number analysis, 5-7 mm thick paraplast embedded brain sections were used. Tissue sections were stained with histological stains, such as Haematoxylin-Eosin (H&E, Merck) and Cresyl Violet (Nissl), or incubated with primary antibodies against GAD67 (mM, 1:1000, Chemicon), GFAP (pRb, 1:200, DAKO), Iba1 (pRb, 1:1000,

Wako), Mac3 (mRat, 1:400, Pharmingen), NeuN (mM, 1:100, Chemicon), NRG1 (Sc-348, pRb, 1:500, Santa Cruz Biotechnology) for DAB based immunostaining (Dako-$LSAB_2$ kit was used according to manufacturer's instructions). Digital images of stained sections were obtained using Zeiss 510-meta LSM (Zeiss, Germany), Axiophot (Zeiss, Germany), DMRXA (Leica, Germany) microscopes. All images were processed with Photoshop CS3, Illustrator CS3 software (Adobe), ImageJ [NIH, Bethesda, USA, (http://rsbweb.nih.gov/ij)] and Fiji (http://fiji.sc/wiki/index.php/Fiji).

Electrophysiology. For slice preparation, mice (10-12 weeks old) were deeply anesthetized with isofluran before decapitation. The brain was quickly removed and immersed for 2-3 min in ice-cold cutting solution (3 mM KCl, 1.25 mM NaH_2PO_4, 6 mM $MgSO_4$, 26 mM $NaHCO_3$, 0.2 mM $CaCl_2$, 10 mM Glucose, 218 mM Sucrose). Transverse slices (300 µm) were cut with a vibroslicer and transferred to recording chamber that was continuously perfused with artificial cerebrospinal fluid (ACSF; 126 mM NaCl, 3 mM KCl, 1.25 mM NaH_2PO_4, 1 mM $MgSO_4$, 26 mM $NaHCO_3$, 2 mM $CaCl_2$, 10 mM Glucose, aerated with 95% O_2 and 5% CO_2 (3-4 ml/min).

Field recording electrodes were pulled from thin-walled borosilicate glass capillaries and filled with ACSF. Extracellular field potential recordings were done using a custom built DC amplifier. Data were digitized by a DigiData 1322A (Molecular Devices, Sunnyvale, CA, USA). Initial data analysis was done in Clampfit 10.0 (Molecular Devices, Sunnyvale, CA, USA). The stimulation electrode was placed in stratum radiatum at the CA3/CA1 junction for the activation of Schaffer collaterals. The recording electrode was placed in the stratum radiatum of the CA1 region. The magnitude of fEPSPs was measured as amplitude (baseline to peak) and slope (20-80% level of the falling phase). Baseline fEPSCs were set to about 50% of maximum responses. LTP was induced by three trains separated by 20 s, each train consisting of 100 Hz stimulation for 1s. Post-train responses were measured every 20 s for 60 min. fEPSPs were filtered by a four-pole Bessel filter at a corner frequency of 2 kHz, and digitized at a sampling rate of 20 kHz using the DigiData 1400A interface (Molecular Devices, Sunnyvale, CA).

For whole-cell patch recordings, acute transverse hippocampal or cortical slices (300 µm) were prepared as described above. All recordings were performed in CA1 pyramidal neurons or cortical layer V projection neurons. The extracellular solution was as for LTP experiments. Pipette solution contained 140 mM KCl, 1 mM $CaCl_2$, 10 mM EGTA, 2 mM $MgCl_2$, 4 mM Na_3ATP, 0.5 mM Na_3GTP, 10 mM HEPES, pH 7.3. Spontaneous inhibitory PSCs were recorded at a holding potential of -70 mV in the presence of 10 µM CNQX and 40 µM AP5. Spontaneous excitatory PSCs were recorded at a holding potential of -70 mV in the presence of 5 µM strychnine and 5 µM bicuculline. For mIPSCs and mEPSCs recordings, 0.5 µM TTX was added to the bath solution. Signals with amplitudes of at least two times above the background noise were selected. Patches with a serial resistance of >10 MΩ, a membrane resistance of <0.2 GΩ, or leak currents of >200 pA were excluded. Data acquisition and analysis were done using commercially available software: pClamp 10.0 (Molecular Devices, Sunnyvale, CA), MiniAnalysis (SynaptoSoft, Decatur, GA) and Prism 4 (GraphPad, San Diego, CA). Statistical significance was evaluated using two-tailed unpaired Student's t-test, with or without Welch's correction or non-parametric Mann–Whitney tests, depending on the distribution of the data. Significance level was set to $P<0.05$. Numerical values are represented as mean±standard error. Data are presented as plots of cumulative probability.

***In vivo* stimulated emission depletion (STED) nanoscopy**: STED nanoscopy was performed as acute experiments; mice were sacrificed after imaging by an overdose of anesthetics. General anesthesia was initiated by pentobarbital injection (60-80 mg/kg body weight; i.p) and continued by infusion of ethohexital (40-60 mg/kg body weight and hour; i.v). To avoid movements by active respiration, mice were paralyzed with pancuronium (800 µg/kg body weight and hour, i.p.) and artificially ventilated at 100-120 stokes/min and 100-140 µl/stroke after insertion of a tracheal tube **(Berning et al., 2012).** A pedestal to fix the head was glued to the scull above the olfactory bulb, while the coverslip was glued on a circular hole upon the visual cortex. Body temperature was kept constant (36°C-38°C) throughout the experiment. For technical details regarding STED imaging see supplementary material in **(Berning et al.,**

2012). Image processing was performed using ImageJ or Fiji. For quantification of dendrites and spines, the “Simple Neurite Tracer” macro (Fiji) was used.

***In vivo* two-Photon laser scanning microscopy (2P-LSM):** Acute 2 photon imaging was performed under general anesthesia using a gas mixture of O_2:N_2O (1:1) loaded with 5% isoflurane in a closed box (flow rate: 1000 ml/min). Following initial sedation, anesthesia was applied by a mask on a heated plate and reduced flow rate (N_2O: 100-200 ml/min; O_2: 200-300 ml/min; 1.5-2% isoflurane). The respiration rate was kept below 2 per second by adjusting the isoflurane dosage and the body temperature was kept constant (36°C-38°C) throughout the experiment **(Agarwal et al., 2011)**. During imaging the skull was attached to a custom-made ring by dental cement to reduce movements. A cranial window through the parietal bone was produced inside the ring close to the sagittal suture. The exposed cortex was covered by a glass coverslip. The structural imaging was carried out by a custom-made microscope equipped with a fs-pulsed titanium-sapphire laser (Chameleon Vision II; Coherent, Glasgow, UK) and a long-distance W Plan-Apochromat 20x/1.0 water immersion objective (Zeiss; Jena, Germany). For excitation, the laser was set at 925±5 nm, and fluorescent signal was collected by a photo-multiplier tube (Hamamatsu, Japan) through a 510±42 nm band pass filter (Semrock). Uniformly spaced (0.8-2 µm) planes of 125x125 to 500x500 μm^2 regions of the cerebral cortex were recorded and processed to obtain z-stacks of images (512x512 or 1024x1024 pixels in size). Image processing was performed using Matlab (version 7, MathWorks, Ismaning, Germany) and ImageJ or Fiji.

Behavioral testings:

Open field: Spontaneous activity of *CK-Cre*Nrg1$^{f/f}$*, *CK-Cre*Nrg1$^{f/+}$ and Nrg1$^{f/+}$* mice was tested in a grey Perspex arena (120 cm in diameter, 25 cm high). Mice were placed in the center and allowed to explore for 7 min. Behavior was recorded by a PC-linked overhead video camera. Viewer software was used to calculate distance traveled and time spent in the central, intermediate or peripheral zones of the open

field. Locomotor activity and anxiety of *HA-Nrg1-tg* (males n=16, females n=10) and WT mice (males n=18, females n=18) were assessed in an open-field test using a Plexiglas box (45 x 45 x 55 cm). Mice were placed individually and allowed to explore for 10 min. Infrared sensors monitored the time spent in distinct areas of the arena (center, 70% of total area; periphery, 30%), distance travelled and rearings. Data were analyzed using ActiMot software (TSE, Bad Homburg, Germany).

Cued and contextual fear conditioning: Fear conditioning was performed as described **(Radyushkin et al., 2005)**. Briefly, mice were trained within the same session for both contextual and cued fear conditioning. Training consisted of exposing mice for 120 s to the context to assess baseline activity. This period was followed by a 10 s, 5 kHz, 85 dB tone (conditioned stimulus, CS). Immediately after the tone, a 2 s, 0.4 mA foot shock (unconditioned stimulus, US) was applied. This CS-US pairing was repeated 13 s later. All mice remained in the conditioning chamber for an additional 23 s following the second CS–US pairing. The contextual memory test was performed 48 h after training. Mice were monitored over 2 min for freezing in the same context as used for training. The cued memory test was performed 52 h after training in a new chamber. First, mice were monitored for freezing over a 2 min pre-cue period with no tone to assess freezing in the new context. Next, a 2 min cue period followed in which the tone was presented. Duration of freezing behavior, defined as the absolute lack of movement (excluding respiratory movements), was recorded by a video camera and a PC equipped with 'Video freeze' software (MED Associates, St. Albans, Vermont, USA).

MK-801 treatment: MK-801 was dissolved in saline and injected i.p. (0.3 mg/kg; volume of injection, 0.1 ml/10 g body weight). Distance travelled in the open field was recorded as described above. Baseline activity (i.e. distance travelled) was determined over 4 min time intervals for 20 min before injection. Effect of MK-801 was measured for 120 min following injection. Again, travelled distance was determined over 4 min time intervals. MK-801 induced changes in activity were expressed for each mouse as percentage of individual baseline.

Prepulse inhibition: Mice were placed in cylindrical enclosures equipped with an ultra-sensor for movement recording located in sound-attenuating cabinets (SR-LAB^{TM}, San Diego Instruments). An experimental session included (I) a 3 min habituation to the set-up and 65 dB background white noise present continuously throughout the entire experiment and (II) a test session as described previously **(Brzozka et al., 2010)**. First, six pulse-alone trials of 120 dB intensity and 40 ms duration were applied to minimize influence of within-session habituation (data not included in PPI analysis). The startle reaction to an acoustic stimulus was recorded for 80 ms starting with the onset of the stimulus. For PPI testing, the 120 dB startle pulse of 40 ms duration was applied either alone or 100 ms after a presentation of a non-startling prepulse stimulus of 70, 75 or 80 dB intensity and 20 ms duration. Different trials (10 of each type) were applied with inter-trial intervals alternating from 8 to 22 s in a pseudorandom order. PPI was calculated as follows: prepulse inhibition (%) = 100 - [(startle amplitude after prepulse and pulse) / (startle amplitude after pulse only)×100] (for details see: **(Brzozka et al., 2010)**).

Supplemental References

Agarwal, A., Dibaj, P., Kassmann, C.M., Goebbels, S., Nave, K.A., and Schwab, M.H. (2011). In Vivo Imaging and Noninvasive Ablation of Pyramidal Neurons in Adult NEX-CreERT2 Mice. Cereb Cortex.

Berning, S., Willig, K.I., Steffens, H., Dibaj, P., and Hell, S.W. (2012). Nanoscopy in a living mouse brain. Science (New York, NY 335, 551.

Brzozka, M.M., Radyushkin, K., Wichert, S.P., Ehrenreich, H., and Rossner, M.J. (2010). Cognitive and sensorimotor gating impairments in transgenic mice overexpressing the schizophrenia susceptibility gene Tcf4 in the brain. Biological psychiatry 68, 33-40.

Chen, Y.J., Johnson, M.A., Lieberman, M.D., Goodchild, R.E., Schobel, S., Lewandowski, N., Rosoklija, G., Liu, R.C., Gingrich, J.A., Small, S.*, et al.* (2008). Type III neuregulin-1 is required for normal sensorimotor gating, memory-related behaviors, and corticostriatal circuit components. J Neurosci 28, 6872-6883.

Deakin, I.H., Nissen, W., Law, A.J., Lane, T., Kanso, R., Schwab, M.H., Nave, K.A., Lamsa, K.P., Paulsen, O., Bannerman, D.M., and Harrison, P.J. (2011). Transgenic Overexpression of the Type I Isoform of Neuregulin 1 Affects Working Memory and Hippocampal Oscillations but not Long-term Potentiation. Cereb Cortex.

Dodd, P.R., Hardy, J.A., Oakley, A.E., Edwardson, J.A., Perry, E.K., and Delaunoy, J.P. (1981). A rapid method for preparing synaptosomes: comparison, with alternative procedures. Brain research 226, 107-118.

Gerlai, R., Pisacane, P., and Erickson, S. (2000). Heregulin, but not ErbB2 or ErbB3, heterozygous mutant mice exhibit hyperactivity in multiple behavioral tasks. Behavioural brain research 109, 219-227.

Jiang, L., Emmetsberger, J., Talmage, D.A., and Role, L.W. (2013). Type III neuregulin 1 is required for multiple forms of excitatory synaptic plasticity of mouse cortico-amygdala circuits. J Neurosci 33, 9655-9666.

Luo, X., He, W., Hu, X., and Yan, R. (2013). Reversible Overexpression of Bace1-Cleaved Neuregulin-1 N-Terminal Fragment Induces Schizophrenia-Like Phenotypes in Mice. Biological psychiatry.

Mizoguchi, A., Ueda, T., Ikeda, K., Shiku, H., Mizoguti, H., and Takai, Y. (1989). Localization and subcellular distribution of cellular ras gene products in rat brain. Brain Res Mol Brain Res 5, 31-44.

O'Tuathaigh, C.M., Harte, M., O'Leary, C., O'Sullivan, G.J., Blau, C., Lai, D., Harvey, R.P., Tighe, O., Fagan, A.J., Kerskens, C.*, et al.* (2010). Schizophrenia-related endophenotypes in heterozygous neuregulin-1 'knockout' mice. The European journal of neuroscience 31, 349-358.

Radyushkin, K., Anokhin, K., Meyer, B.I., Jiang, Q., Alvarez-Bolado, G., and Gruss, P. (2005). Genetic ablation of the mammillary bodies in the Foxb1 mutant mouse leads to selective deficit of spatial working memory. The European journal of neuroscience 21, 219-229.

Rimer, M., Barrett, D.W., Maldonado, M.A., Vock, V.M., and Gonzalez-Lima, F. (2005). Neuregulin-1 immunoglobulin-like domain mutant mice: clozapine sensitivity and impaired latent inhibition. Neuroreport 16, 271-275.

Rao, S., Zhou, M., Merker, R., Mann, M., Fischbach, G., and Gingrich, J. (2004). Behavioral alterations in mice with a reduced neuregulin-1 ig domain isoform. In 7th Annual Meeting; International Society for Developmental Psychobiology.

Shamir, A., Kwon, O.B., Karavanova, I., Vullhorst, D., Leiva-Salcedo, E., Janssen, M.J., and Buonanno, A. (2012). The importance of the NRG-1/ErbB4 pathway for synaptic plasticity and behaviors associated with psychiatric disorders. J Neurosci 32, 2988-2997.

Stefansson, H., Sigurdsson, E., Steinthorsdottir, V., Bjornsdottir, S., Sigmundsson, T., Ghosh, S., Brynjolfsson, J., Gunnarsdottir, S., Ivarsson, O., Chou, T.T.*, et al.* (2002). Neuregulin 1 and susceptibility to schizophrenia. Am J Hum Genet 71, 877-892.

Yin, D.M., Chen, Y.J., Lu, Y.S., Bean, J.C., Sathyamurthy, A., Shen, C., Liu, X., Lin, T.W., Smith, C.A., Xiong, W.C., and Mei, L. (2013). Reversal of behavioral deficits and synaptic dysfunction in mice overexpressing neuregulin 1. Neuron 78, 644-657.